International Journal of Heat and Fluid Flow 91 (2021) 108812

Contents lists available at ScienceDirect

International Journal of Heat and Fluid Flow

journal homepage: www.elsevier.com/locate/ijhff

Swirl number and nozzle confinement effects in a flat-vane axial swirler

I.V. Litvinov [a,b,*], D.A. Suslov [a,b], E.U. Gorelikov [a,b], S.I. Shtork [a,b]

[a] Kutateladze Institute of Thermophysics, Novosibirsk, Russia
[b] Novosibirsk State University, Novosibirsk, Russia

ARTICLE INFO

Keywords:
Flat-vane axial swirler
Swirl number
Precessing vortex core
PVC
Central recirculation zone
CRZ
Strouhal number
Pressure pulsations
LDV
Microphone

ABSTRACT

This paper presents the results of a parametric experimental study of free swirling flow at the exit of a flat-vane axial swirler. A total of 16 data sets were acquired by combining four swirler vane angles (22°, 29°, 50.5°, and 58.3°) and four exit nozzles of different diameters (30, 40, 52, and 76 mm). Sophisticated pressure probes consisting of precise microphones and a two-component LDV system were used to investigate the effect of these geometrical parameters on swirling flow regimes characterized by the swirl number. Particular attention was paid to the precessing vortex core (PVC) phenomenon observed at the exit of the swirler nozzle. It has been shown that by varying the vane angle and the diameter of the exit nozzle, it is possible to independently control the swirl number value and the occurrence of a PVC. A distinct correlation has been found between the PVC-induced pressure pulsations detected by acoustic probes and the tangential velocity fluctuations measured by LDV. The use of microphones provides a quick way to measure the frequency response of swirl flow in a wide range of geometries and flow configurations. The PVC effect does not occur at low subcritical values of the integral swirl number ($S < 0.5$) and in the case of strong swirl flow ($S_g = 0.9$ and 1.2) in the absence of constriction by the nozzle ($D_e/D_0 = 1$). The disappearance of the PVC effect for strong swirl flow without constriction is due to the extreme displacement of the flow to the nozzle walls. The absence of a PVC in the flow was inferred not only from measurements of the frequency response of the flow over a wide range of *Re* numbers, but also from the absence of specific markers in velocity RMS distributions. Measurement results are used to derive an empirical correlation of the integral swirl number and the Strouhal number with a modified geometric swirl number. This allows a generalization of the frequency characteristics of swirling flows with a PVC for flat-vane axial swirlers, which are widely used in engineering.

1. Introduction

Swirling flows are widely used in various fields of science and technology. For example, flow swirling is a simple way to stabilize combustion (Syred and Beer, 1974). This is achieved through the formation of a central recirculation zone (CRZ), which returns the combustion products to the primary flame zone, thus maintaining stable combustion. As a rule, the formation of a CRZ is accompanied by an unsteady vortex phenomenon referred to as the precessing vortex core (PVC) (Gupta et al., 1984; Syred, 2006). In this case, the center of the vortex performs a precessional motion around the center of flow symmetry, generating regular pressure pulsations (Martinelli et al., 2007). Moreover, it has been found that the recirculation zone is not stationary and axisymmetric with respect to the center (Yazdabadi et al., 1994). The CRZ moves coherently with the PVC and rotates at the same frequency (Syred et al., 1975; Syred, 2006; Litvinov et al., 2013, 2019).

As shown in classical experimental studies of the PVC (Chanaud, 1965; Cassidy and Falvey, 1969), the precession frequency is a linear function of the flow rate. Recently, the 3D left-handed spiral (helical) geometry of the PVC has been clearly demonstrated in a number of studies (e.g. Cala et al., 2006; Oberleithner et al., 2011; Stöhr et al., 2011; Dulin et al., 2019) under reacting and isothermal conditions. The precession frequency does not coincide with the local frequency of flow rotation due to the effect of self-induced motion generating a reverse flow along the vortex chamber axis (Cassidy and Falvey, 1969; Alekseenko et al., 1999; Anacleto et al., 2003).

The PVC phenomenon has a significant effect on the flow by generating unwanted vibrations and noise (Pausch et al., 2020). Experiments have shown that the simultaneous presence of acoustic oscillations and the helical mode gives rise to a strong nonlinear interaction, which manifests itself in an oscillation component at the difference between the acoustic and flow frequencies (Boxx et al., 2010). There is also a risk

* Corresponding author.
E-mail address: litvinov@itp.nsc.ru (I.V. Litvinov).

https://doi.org/10.1016/j.ijheatfluidflow.2021.108812
Received 11 September 2020; Received in revised form 29 January 2021; Accepted 23 March 2021
Available online 5 August 2021

of resonance with the natural frequencies of the installation (Candel et al., 2014). In addition, the PVC in cyclones not only generates strong vibrations of the equipment, but can also reduce the particle separation efficiency (Derksen and Van den Akker, 2000; Yang et al., 2019). When a hydro turbine operates in partial load regimes, the PVC or "vortex rope" effect is also highly undesirable because it generates strong periodic pressure pulsations propagating through the water column from the draft tube (Ciocan et al., 2007; Iliescu et al., 2008; Goyal et al., 2017; Pasche et al., 2017; Rajan and Cimbala, 2017; Mohammadi et al., 2019). In this regard, it is very important that the emergence of the PVC and its associated pressure pulsations in technical equipment be accurately predicted at the design stage.

The determining parameters of single-phase and incompressible swirling flows, according to (Grimble and Agarwal, 2015), are the *Reynolds* number $Re = UD_V/\nu$ and the swirl number $S_V = \frac{\Omega D_V}{U}$ (here Ω is the angular velocity of rotation of the model vortex, D_V is the vortex size, U is the velocity scale, and ν is the kinematic viscosity). A dimensionless parameter that characterizes self-oscillating flow with a certain PVC frequency f is the *Strouhal number* $Sh = \frac{f D_V}{U}$. According to the Buckingham π theorem, the Sh number is a definable parameter that depends on the Reynolds number Re, the swirl number S, and dimensionless combinations of the geometric dimensions of the vortex chamber X_i. Then the final criterion relation can be written as $Sh = F(Re, S, X_i)$

The difficulty of describing vortex flows is that often such an empirical relation determined for a given vortex chamber geometry may not be valid for other devices.

The classical definition of the integral swirl number is given in (Gupta et al., 1984):

$$S_{int} = \frac{G_\theta}{RG_z},$$
$$G_\theta = \int_0^\infty (\rho V_{ax} V_{\text{tang}} + \rho v'_{ax} v'_{\text{tang}}) r^2 dr, \quad (1)$$
$$G_z = \int_0^\infty (\rho V_{ax}^2 + \rho v_{ax}'^2 + (p - p_\infty)) r dr,$$

where v_{ax} and v_{tang} are the axial and azimuthal velocity components, $()'$ is the pulsating velocity component, R is the radius of the tube or nozzle, and p-p_∞ denotes the pressure difference between the swirling jet and the fluid at rest. Various critical aspects of this definition such as the influence of the velocity distribution (Farokhi et al., 1989) or the contribution of the pressure part (Degenève et al., 2019) were addressed in the literature. Since it is difficult to measure the distributions of pressure and velocity fluctuations, the swirl number is often calculated neglecting their contributions to the swirl number (Sheen et al., 1996; Toh et al., 2010; Skripkin et al., 2016). Then the integral swirl number can be calculated by the simplified formula

$$S = \frac{\int_0^R V_{ax} V_{\text{tang}} r^2 dr}{R \int_0^R V_{ax}^2 r dr} \quad (2)$$

The definition of the swirl number in the form (2) is not convenient for engineering calculations as it is necessary to accurately measure the distribution of two velocity components along the vortex chamber. The literature describes a large number of different swirling devices, the properties of the flows produced by such devices, and various definitions of the swirl number suitable for a particular type of swirler (Milosavljevic et al., 1990; Sheen et al., 1996; Cala et al., 2006; Syred, 2006; Toh et al., 2010; Durox et al., 2013; Grimble and Agarwal, 2015). Most often, this parameter is defined as the ratio of the tangential velocity component to the axial one. However, in practice, it is common to use geometric definitions of the swirl number, which allow one to calculate the swirl number without measuring the exit velocity profile and to predict, e.g., the formation of a PVC in the flow (Syred, 2006).

Three types of geometries are typically used to create swirling flows: radial swirlers with blades, axial vane swirlers with flat or profiled blades, and swirlers with tangential injection (cyclone type) inlets.

For radial swirlers with blades, the following expression was proposed (Sheen et al., 1996):

$$S_g = C(Re)\cdot\sigma(\varphi), \quad \text{where} \quad \sigma(\varphi) = \frac{1}{1-\psi}\left(\frac{tan\varphi}{1+tan\varphi tan(\pi/z)}\right) \quad \text{and}$$

$\psi = zs/(2\pi R cos\varphi)$. Here z is the number of guide vanes, s is the blade width, R is the inner radius of the swirler, and φ is the vane angle. The design swirl parameter of cyclone (tangential) swirlers is determined according to the formula $S_g = \pi D D_0/(4A_T)$, where D and D_0 are the diameters of the outlet nozzle and the main part of the cyclone chamber, respectively, and A_T is the area of tangential inlet nozzles (Syred, 2006). The degree of swirl for vane swirlers can be characterized using the following geometric swirl number (Chigier and Beér, 1964; Gupta et al., 1984):

$$S_g = \frac{2}{3}\left(\frac{1-(d/D_0)^3}{1-(d/D_0)^2}\right) tan(\varphi) \quad (3)$$

here d and D_0 are the diameters of the hub and the swirler and φ is the vane angle. It is known that the geometric swirl number calculated using formula (3) can exceed the integral swirl number by a factor as large as two (Candel et al., 2014). Nevertheless, the geometric definition is common in the literature as it is easy to use in engineering design (Hee Lee et al., 2002; Khandelwal et al., 2014; Balakrishnan and Srinivasan, 2018). The lack of a universal swirl number not only hinders comparison of flow characteristics from different studies, but can also lead to major differences in understanding the phenomenon.

It was reported (Chigier and Chervinsky, 1967) that when the swirl number reached a value of 0.6, a PVC formed in the flow. This implies that the mean velocity distribution at the swirl exit has a major influence on the development of hydrodynamic instability in the form of vortex breakdown, and the distribution, in turn, substantially depends on the method of imparting swirl to the flow. In previous studies (Syred, 2006; Litvinov et al., 2019; Manoharan et al., 2020), vortex breakdown in the form of a PVC has been identified in various swirl flows at sufficiently high swirl numbers and Reynolds numbers. In fact, this implies that the swirl number is the main criterion for the formation of PVC; yet it has no rigorous definition.

In addition, as noted above, in the case of vortex breakdown of the PVC type, literature data on the Strouhal number Sh as a definable parameter of the swirl number S are limited and contradictory. In (Al-Abdeli and Masri, 2004; Dinesh and Kirkpatrick, 2009), the nondimensional precession frequency (Sh number) is found to be a drooping curve function of swirl number in the Sydney burner model considered. Zakharov et al. (2014) reported a linear increase in Sh as a function of swirl number for a radial swirler. The effect of an extraordinary non-monotonic evolution of the Strouhal number vs. the Swirl number, with a region of an inverted (decreasing) dependence was observed by Shtork et al. (2008) under both isothermal and reacting conditions. Grimble and Agarwal (2015) performed an empirical analysis of the Strouhal number based on parametric data. For a cyclone of a particular shape, it is shown that the best-fit curve for the Strouhal number is $Sh \sim S_g^{-0.71}(\frac{D_e}{D})^{2.15}$, where D_e/D is the ratio of the outer and inner diameters of the cyclone.

In this work, we carried out a parametric study of the PVC effect for flat-vane axial swirlers. A clear link was found between the pressure pulsations due to a PVC and the tangential velocity fluctuations measured by LDV. The use of microphones provides a quick way to measure the frequency response of the swirl flow in a wide range of geometries and flow configurations. It is shown that by varying the vane angle and the diameter of the exit nozzle, it is possible to independently influence the swirl number and the formation of a precessing vortex core (PVC) at the exit of the swirler nozzle. The degeneration of the PVC effect in the case of strong swirling flow in the absence of constriction by

the nozzle is shown for the first time. In addition, we attempted to find an empirical correlation $Sh(S)$ for axial vane swirlers. This problem is highly relevant for for the prediction of the frequency characteristics of flows with PVC formation in engineering applications.

2. Experimental setup

2.1. Flat-vane axial swirler

The experiments were carried out on an aerodynamic rig, which included a blower with a flow rate of up to 550 m^3/h, an ultrasonic flow meter, a frequency converter, an aerosol generator, and a test section (see Fig. 1).

The test section is an axisymmetric vane swirler. The upstream section is a pipe with smooth walls 105 mm in diameter and 1.5 m long. Flow is swirled by vanes mounted in the annular gap. Next, the flow is constricted to the center using nozzles of various diameters. We used four replaceable vane swirlers with vane angles of $\varphi = 22^\circ$, 29°, 50.5°, and 58.3° and different replaceable exit nozzles with diameters $D_e = 30$, 40, 52, and 76 mm. The remaining dimensions are shown in Fig. 1. The degree of swirl for this type of vane swirler can be characterized using the geometric swirl number based on (3): $S_g = \frac{2}{3}\left(\frac{1-(d/D_0)^3}{1-(d/D_0)^2}\right)tan(\varphi)$, where $d = 30$ mm and $D_0 = 76$ mm are the diameters of the hub and the swirler, and φ is the vane angle (Fig. 1). Thus, under our conditions, the geometric swirl number calculated by formula (3) took values of 0.3, 0.6, 0.9, and 1.2. The parameters d, D_0, and L are fixed in this study. According to (Akhmetov et al., 2004), when the chamber length L (in our case, it is the nozzle length) is reduced by a factor of about 2.5, the values of Sh vary by not $>$ 15%. Due to this, we do not consider the variation of this parameter.

This study focused mainly on the flow structure in the near field region of the swirling jet and was performed under unconfined conditions. For practical installations such as vortex burners, it is neceesary to consider the impact of the combustion chamber on the flow. As regards sudden expansion configurations similar to those used in the present study, previous studies have confirmed that the vortex flow characteristics in the vicinity of the dump plane are insensitive to the confinement effect, especially for expansion ratios above 2.2 typical of gas turbine combustion chambers (Anacleto et al., 2003). Obviously, the confinement effect can be significant at large D_e comparable to the diameter of the combustion chamber, but a thorough analysis of this issue is beyond the scope of the present paper.

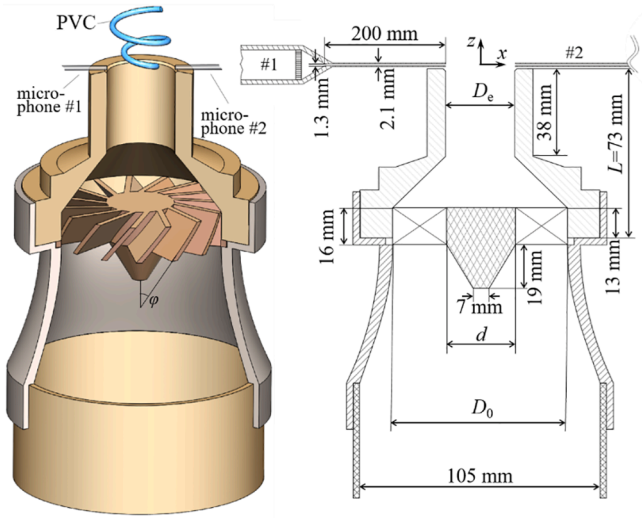

Fig. 1. Sketch of the test section – flat-vane swirler.

3. Experimental measuring techniques

The air flow was set and controlled with an error of 1.5% using the blower, the frequency converter, and the ultrasonic flow meter. The Reynolds number $Re = U_0 \cdot D_e/\nu$, determined from the exit nozzle diameter D_e and the flow-averaged velocity U_0, was varied from 10^4 to $5 \cdot 10^4$. The experiments were performed with atmospheric air at room temperature. The additional uncertainty in the calculation of Reynolds numbers associated with the change in air viscosity due to fluctuations in ambient temperature is assumed to have a minor influence on the conclusions drawn from the work since the flow characteristics are weakly dependent on Re.

The regular pressure pulsations generated by the PVC effect were recorded using two Behringer ECM8000 microphones located on opposite sides of the swirler nozzle (Fig. 1). To reduce the effect of the microphones on the flow, we used tiny pressure taps in the form of a thin tube 150 mm long and 2 mm in diameter. Such pressure taps change the amplitude and phase of the measured signal, but do not affect the determination of the PVC frequency. The PVC frequency was determined from the difference signal between two sensors. When the vortex precesses, alternately approaching one or the other of the sensors, the sensor signals are recorded in opposite phases (Gursul, 1996; Fernandes et al., 2006). Therefore, signal subtraction makes it possible to enhance the out-of-phase component and remove the in-phase aerodynamic noise not related to PVC motion. The PVC frequency f_{PVC} was determined as the frequency of the maximum peak in terms of the power spectral density (PSD) obtained by a fast Fourier transform (FFT) of the difference signal (p_1-p_2) records. The measured PVC frequencies f_{PVC} were in the range 30–500 Hz. Thus, the Strouhal number Sh, defined as $f_{PVC} \cdot D_e/U_0$, varied in the range 0.5–1.0. In an automated experiment (swipe mode), the flow rate Q, m^3/h was varied from 10 to 150 m^3/h in increments of 0.14 m^3/h, with a difference signal of 1 s duration recorded with a sampling frequency of 2 kHz at each point. Thus, for each flow configuration, we obtained the dependence of the precession frequency f_{PVC} on the flow rate with a total number of points of about 10^3. The standard deviation of the points from the average linear dependence $f_{PVC}(Q)$ determines the uncertainty associated with the determination of the PVC frequency. As regards the accuracy of measuring the PVC frequency at a local measuring point, it is determined by the statistics collection time of 1 s; therefore, the uncertainty in determining the PVC frequency was 1 Hz. This relatively low resolution was a compromise to provide coverage of a wide range of flowrates in order to obtain a better resolution of the precession frequency as a function of flowrate in the time required for data acquisition.

Velocity distributions at the exit of the swirler nozzle were measured using a LAD-06-i two-component laser-Doppler anemometer (LDA) with the addition of tracers (small particles of vegetable oil with a diameter of 1 μm) to the flow. Tracers were generated by a Laskin atomizer (Tropea et al., 2007). Velocity profiles were measured at the minimum possible distance to the nozzle of the swirler equal to 3 mm. Velocity distributions in the x-z section were measured at points spaced at intervals of 2 mm along the x axis and every 5 mm along the z axis. Points in the velocity profiles (along the x axis, y, $z = 0$) were located every 1 mm. The positioning system could position the measuring volume of the LDA with linear dimensions of 0.005x0.8 mm with an accuracy of 0.1 mm, which provided good resolution of velocity gradients in our survey (≈1 m/s per 1 mm). In measurements of the mean velocity, the certified accuracy of the LAD-06i device is 0.5% of the measured value. The error of the mean velocity and the standard deviation from the mean velocity in turbulent flow ($Re > 10^4$) with high velocity pulsations was estimated according to (Yanta and Smith, 1978). To measure the average velocity in turbulent flow with a 95% confidence, it is necessary to collect statistics on the number of LDA bursts of about $1600\left(\sqrt{U^2}/\langle U\rangle\right)^2$, i.e. the required number of LDA bursts depends on the local velocity values of the sample:

the mean value and the standard deviation. In the experiments, the average number of LDA bursts was $5{\cdot}10^3$ per one velocity component, the maximum measurement time at a point was ~ 60 sec, and the average particle density was $\approx 10^3$ bursts per second. The minimum number of measurements (about 10^3) was made in regions with a few tracers – behind the nozzle of the swirler. Nevertheless, even in these regions, the reliability of determining the mean velocity was at the 95% level. For a prescribed error, the number of measurements for determining the standard deviation of the velocity is $^2/_{error^2}$ (Yanta and Smith, 1978). Moreover, the expression does not depend on the local characteristics of the sample. In the experiments, the error of the standard deviation of the velocity was within 2%. LDA velocity data were recorded simultaneously with microphone signals to perform phase average measurements according to the PVC phase.

4. Results

4.1. Mean and RMS velocity distributions of the flow with PVC

In the first stage of the study, we proved that the velocity distributions did not depend on the flow regime (*Re* number), i.e., self-similarity took place (Gupta et al., 1984; Valera-Medina et al., 2009; Litvinov et al., 2013). The axial and tangential velocity profiles also show that the flow characteristics are independent of the *Re* number (Fig. 2). Here the velocity profiles are made dimensionless by dividing by the velocity U_0 (D_e = 52 mm, S_g = 0.6).

Starting at $Re \approx 10^4$, the distributions of the mean velocity divided by the flow-averaged velocity U_0 become self-similar, indicating a weak dependence of the flow structure on the Reynolds number. Deviation from self-similarity takes place only at low *Re* parameters, and this reflects the occurrence of the transition process associated with the development of a breakdown zone and the formation of a PVC (Gupta et al., 1984).

Velocity profiles for all (16) flow configurations (S_g = 0.3–1.2 and D_e = 30–76 mm) were measured for a fixed value $Re = 1.5{\cdot}10^4$ corresponding to the self-similar region. Averaged profiles of the axial and tangential velocities are presented in Fig. 3. It is evident that there is a variety of different axial velocity profiles: with the formation of an extensive CRZ, with a small velocity dip at the center, and almost uniform profiles. The tangential velocity profiles show that the swirl intensity also varies significantly. In this case, both parameters (swirler vane angle and the diameter of the exit nozzle) affect the velocity profiles.

To give an idea of the turbulence field, Fig. 4 show profiles of the root mean square (RMS) fluctuations of the axial and tangential velocity components for the same flow regimes and with the same legend as in Fig. 3. Typical RMS distributions with PVC footprints are observed for the case D_e = 40 and 52 mm (Fig. 4b, c) for all considered swirlers, except for the case of a low swirl number S_g = 0.3. The velocity profiles with a CRZ exhibit pronounced M−shaped RMS profiles of the axial velocity component (Fig. 4, left). It can be seen that the maximum fluctuations of the axial velocity component occur at a distance $r \approx 0.15$–$0.25D_e$ from the jet axis. This location corresponds to the center of the inner shear layer, i.e., the flow surface between the reverse and direct flows. It was also identified that the PVC trajectory is in this region (Gupta et al., 1984; Shtork et al., 2007; Litvinov et al., 2019).

The RMS profiles of the tangential velocity component are marked indicators of the PVC existence (Fig. 4, right). The footprint of PVC motion in the RMS profiles appears as a high central peak and two peaks at the periphery of the flow for the cases D_e = 40 and 52 mm (Fig. 4 b, c) for the all swirlers considered, except for case of a low swirl number S_g = 0.3. The high level of tangential turbulent fluctuations near the center point (x, y, z = 0) in the recirculation zone is induced by the PVC, as shown in (Anacleto et al., 2003; Martinelli et al., 2007). The peak values corresponding to pulsations of the tangential component at this point should be attributed primarily to the inviscid pulsations of the PVC, and to a lesser extent, to stochastic turbulence as the shear in this region is low and turbulence is also damped due to flow rotation in a stable mode (Anacleto et al., 2003; Moeck et al., 2012). This will be proved below by considering the spectrum of the tangential component of velocity pulsations. The central extremum in the RMS distributions of tangential velocity pulsations begins at the lowest swirl intensity in the flow (a, right). This implies that this central extremum is a necessary condition for PVC formation, but it is not a sufficient condition. Two peaks at the periphery of the flow could form if the radius of PVC motion extended to a sufficient distance from the nozzle center, but the absence of two peripheral peaks does not indicate the nonexistence of a PVC.

The case of S_g = 0.6 and D_e = 40 mm (b) is in a transition region of PVC formation. We do not see a distinct M−shaped RMS distribution of the axial component of velocity pulsations and two peripheral peaks in the RMS distribution of the tangential component of velocity pulsations. This implies that the PVC trajectory is at an insufficient distance x/D = 0.1 from the nozzle center. Nevertheless, a PVC is observed for this configuration as will be shown below. Thus, we can state that typical footprints of the PVC in the RMS distributions of velocity pulsations are an M−shaped distribution of the axial velocity component and a central peak of the tangential velocity component.

The RMS profiles of the axial and tangential velocity components do not show the above-mentioned specific markers of the influence of the PVC in the case of low swirl (S_g = 0.3) for all nozzle diameters and in the case of high swirl for a nozzle diameter D_e = 76 mm.

4.2. Frequency response of the flow with a PVC

To determine the conditions under which a PVC occurs at the nozzle exit of the swirler for a wide range of flow rates, the difference signal of pressure pulsations was recorded using two pressure sensors placed diametrically opposite each other at the nozzle edge (Fig. 1) for all 16 variants. Fig. 5 illustrates the pressure spectra (black lines) in terms of the PSD of the difference signal ($p_1 - p_2$) for the cases S_g = 0.3, 0.6, 0.9,

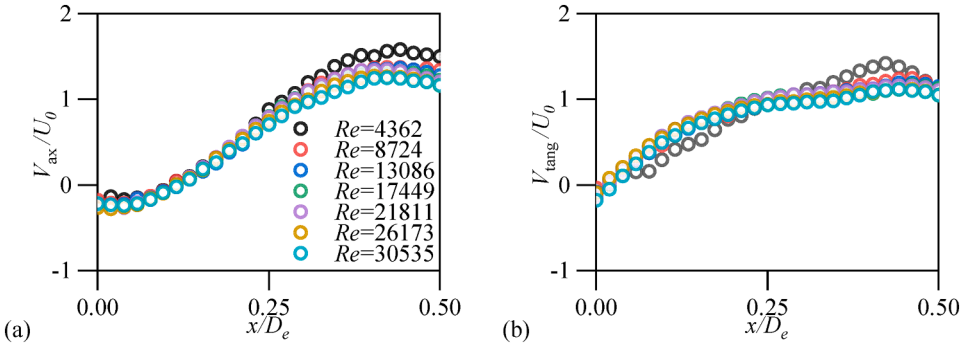

Fig. 2. Independence of velocity profiles on the *Re* number (D = 52 mm, S_g = 0.6).

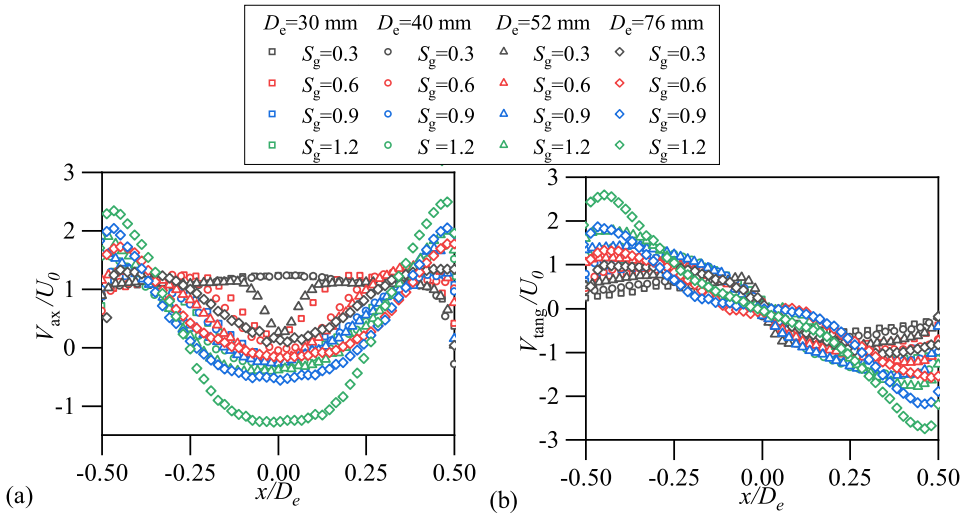

Fig. 3. Axial (a) and tangential (b) velocity profiles for all flow configurations considered ($Re = 1.5 \cdot 10^4$).

and 1.2, respectively at a constant outer diameter of the nozzle $D_e = 52$ mm and fixed $Re = 1.5 \cdot 10^4$. The amplitudes in the spectra were normalized by the maximum value of the dominant peaks. It is seen that there is no distinct peak in the spectrum for the weak swirl case ($S_g = 0.3$) and the dominant peak in the spectra appears in the three cases $S_g = 0.6$, 0.9, and 1.2. The observed pressure peaks were anticipated to be associated with the rotation frequency of the PVC. To prove this, we consider the spectra of the instantaneous tangential velocity component (red) recorded by LDA at the point $x, y, z = 0$.

A comparison of the spectra shows that the peaks of pressure pulsations correlate qualitatively very well with the peaks of velocity pulsations, thus confirming the precessing-vortex origin of the pressure pulsations and the distinct periodic characteristics of precessing motion. There is a clear link between the hydrodynamic fluctuations of the vortex core and the acoustic field produced. This allows us to use microphones as a quicker way to measure the frequency response of swirl flow in a wide range of geometries and flow configurations.

Fig. 6 shows the dependences of the dimensionless PVC frequency in terms of the Strouhal number *Sh* as a function of the Reynolds number. It should be noted that *Sh*(*Re*) as a function is not always monotonic; nevertheless *Sh* is almost independent of *Re*, which has also been noted in previous studies (Cassidy and Falvey, 1969; Grimble and Agarwal, 2015). As we can see from Fig. 6b, the scatter of points for the case $S_g = 0.6$ is much larger than for the other two cases ($S_g = 0.9$ and $S_g = 1.2$). This indicates that for the given nozzle and in the case $S_g = 0.6$, the flow is swirled insufficiently for a pronounced PVC effect.

Table 1 presents the results of identification of a PVC for all 16 flow configurations obtained for four swirl vane angles and four nozzle diameters. The plus (+) and minus (−) signs indicate that a PVC was observed or was not, respectively.

It is evident from the Table 1 that a PVC does not occur at low $S_g = 0.3$ and small nozzles ($D_e = 30$–52 mm). This is most likely due to the subcritical swirl number $S < 0.5$, for which a PVC is not formed in the flow (Gupta et al., 1984). On the other hand, a PVC is not identified for the cases of high swirl intensity $S_g = 0.9$ and 1.2 without a constriction nozzle ($D_e = 76$ mm). These special cases of the absence of a PVC in the flow will be discussed below.

4.3. Footprints of the PVC in the flow

We consider the vertical cross-section along the center of the swirler nozzle in the typical case of the presence of a PVC at high swirl intensity ($D_e = 52$ mm and $S_g = 1.2$). Fig. 8 shows isocontours of the axial $k_{ax}/U_0^2 = < v_{ax}^2 > /U_0^2$ and tangential $k_{tang}/U_0^2 = < v_{tang}^2 > /U_0^2$ contributions of dimensionless turbulent kinetic energy (TKE). It is seen that an extensive CRZ is formed and the location of maximum turbulence generation in the inner shear layer zone coincides with the PVC trajectory which lies at $x \approx 0.3D$ (Fig. 7a). This is explained by the fact that the contribution to TKE is due not so much to turbulent stochastic fluctuations, but to deterministic coherent pulsations caused by the PVC motion. The high level of tangential turbulent fluctuations near the center of the nozzle in the recirculation zone (Fig. 7a) is also induced by the PVC, as shown in (Anacleto et al., 2003; Martinelli et al., 2007). Thus, we can conclude that there are two main footprints of the PVC in the TKE distributions.

To better understand how the PVC effect looks in the crosswise cross-section we consider phase-averaged mean profiles. As a reference signal of phase-averaging with respect to the PVC motion we used the pressure signal from the microphone with a dominant frequency of 84 Hz in the corresponding spectra from Fig. 5. Assuming that the process is quasi-periodic in time and in space, we transform the angle of rotation of the PVC to the azimuthal angle in a cylindrical coordinate system (Cala et al., 2006). Fig. 7b shows how the center of the vortex structure deviates from the central position (Griffiths et al., 1998). The axial velocity maximum is between the vortex core and the nozzle wall, and the region of the reverse flow is also shifted relative to the chamber center. We should note that this is a flow pattern that rotates together with the vortex core.

To understand why the PVC effect does not occur for low swirl numbers, consider the streamlines in Fig. 8, which show that only in the cases $S_g = 0.9$ and 1.2 (c, d), a CRZ does begin to form at the center of the flow, and for the cases $S_g = 0.3$ and 0.6, a CRZ is not observed. The formation of a CRZ is a good indicator of the PVC effect, as is noted in numerous papers (Yazdabadi et al., 1994; Syred, 2006). The maximum in the k_{ax} distributions occurs at a distance $x \approx 0.2$–$0.25D$ from the axis of the chamber nozzle (Fig. 8 c, d), which corresponds to the maximum generation of turbulence in the inner shear layer due to the presence of a PVC. In these two cases, the maximum in the k_{tang} distributions occurs at the center of the flow. This explains why a PVC does not form in these low swirl flows ($S_g = 0.3$ and 0.6, a and b).

Nor does a PVC occur in the opposite case, i.e., when using nozzles of large diameter $D_e = 76$ mm and a swirl number $S_g = 1.2$ (see Table 1.). Although the swirl of the flow far exceeds the subcritical parameter ($S > 0.5$) (Gupta et al., 1984; Syred, 2006), in passing through a large nozzle with a small length-to-diameter ratio, the flow does not have time to change on the path from the swirler to the nozzle exit. Furthermore, the flow turns out to be strongly swirling only at the periphery. In the central part, a relatively weak swirling forced vortex is formed from the air

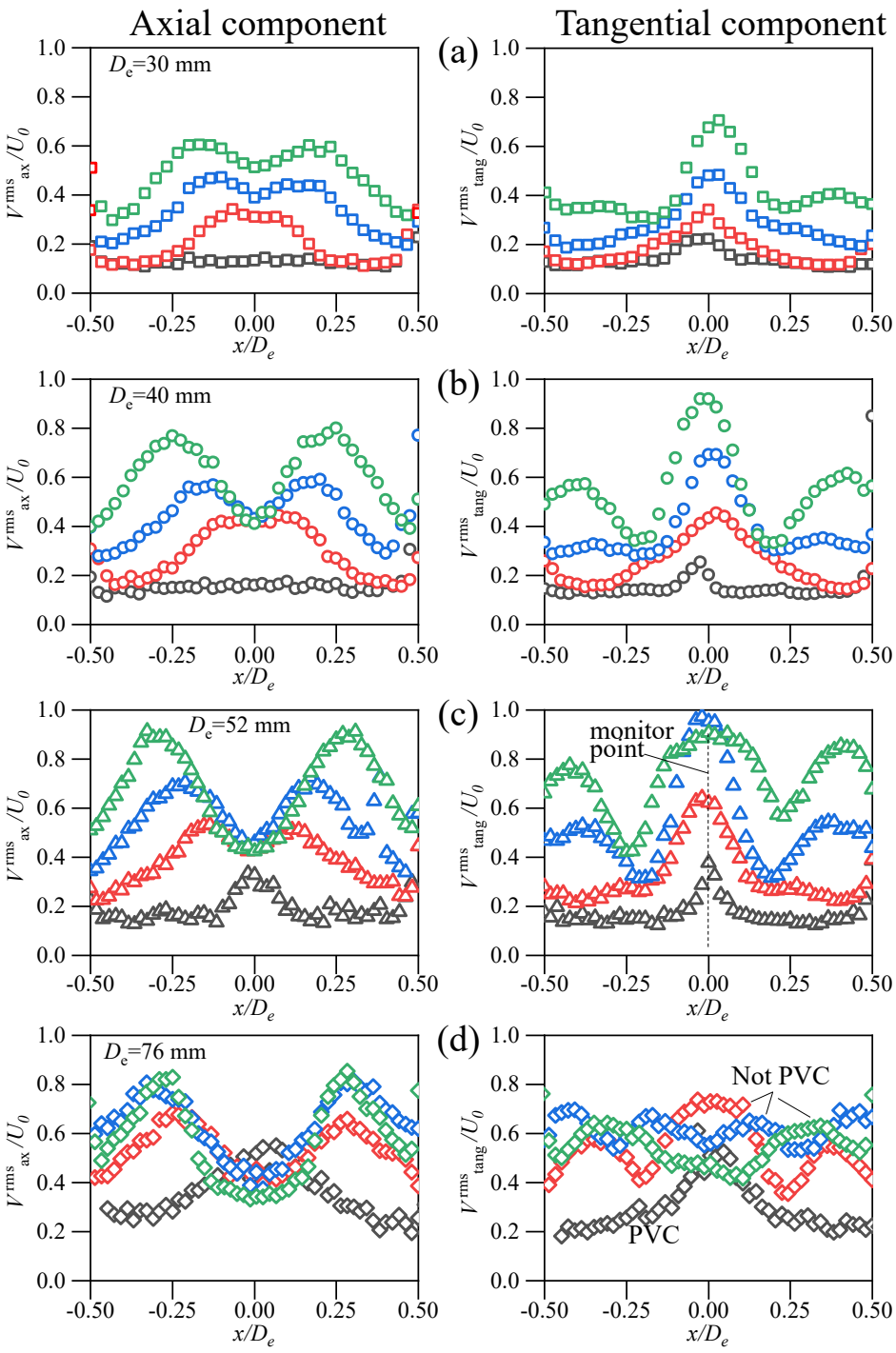

Fig. 4. RMS axial (left) and tangential (right) velocity profiles for all flow configurations considered ($Re = 1.5 \cdot 10^4$): (a) $D_e = 30$ mm, (b) $D_e = 40$ mm, (c) $D_e = 52$ mm, and (d) $D_e = 76$ mm (the same symbols for different S_g as in Fig. 3; the spectra of pulsations from Fig. 5 are recorded in monitor points).

supplied due to the CRZ. Under these conditions, a localized vortex core that can be identified as a PVC is not formed in the flow at the exit of a flat-vane axial swirler.

To gain insight into how the degeneration of the PVC occurs at high swirl numbers $S_g = 1.2$ for $D_e = 76$ mm, we consider the same TKE distributions (Fig. 9). It can be seen that for three nozzle diameters (30, 40, and 52 mm), a PVC occurs in the flow, as is indicated by the corresponding streamline trajectories. It is also seen that the center of the recirculation vortex is shifted lower to the nozzle as the swirl increases. For high swirl numbers $S_g = 0.9$ and 1.2, the CRZ is deep inside the nozzle. This implies that the PVC begins to form immediately behind the swirler due to the high swirl intensity. Next, highly swirled annular flow with a strong CRZ is formed, reaching the height of the nozzle. Nevertheless, the PVC in these regimes is degenerate, and it was not possible to identify it using two microphones for these two regimes ($S_g = 0.9$ and 1.2). The absence of the PVC effect is also indicated by the fact that there is no maximum at the center in the tangential component contribution of TKE (Fig. 9, c, d).

4.4. Swirl number scrutiny

The swirl number was calculated from the measured velocity pro-

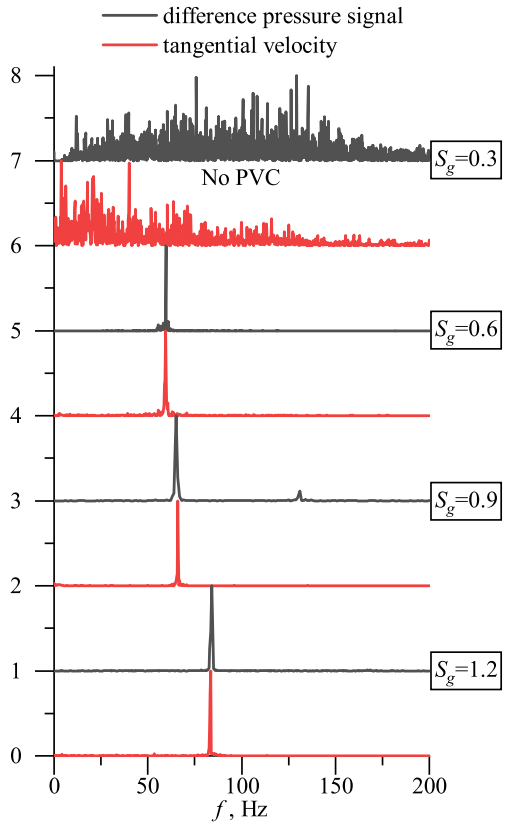

Fig. 5. Comparison of the normalized spectra of pulsations of the pressure difference signal and pulsations of the tangential velocity component ($D = 52$ mm, $Re \approx 1.5 \cdot 10^4$).

files. As a rule, pressure and turbulent pulsations are neglected as in Eq.2. A direct comparison of the integral and geometric swirl parameter is given in (Feikema et al., 1990; Shtork et al., 2005), where it is shown that S is close to S_g for small values $S < 1$. Our results show that this correlation between the geometric and integral definitions of the swirl number is valid only for special cases: 1) $S < 0.6$ and nozzle diameters $D_e = 30$ and 40 mm and 2) $S = 0.9$ and a nozzle diameter $D_e = 76$ mm. The dependence of S on S_g is presented in Fig. 10a, where it can be seen that the measured points S significantly deviate from the linear dependence $S = S_g$. Formula (3) was obtained for conditions corresponding to an exit nozzle diameter of 76 mm (without flow constriction) in our case. For other conditions, this correlation does not hold because of the strong deviation of actual velocity profiles from the model assumptions used in deriving formula (1). To take into account the effect of the constricting nozzle on the swirl number, it is proposed to introduce a modified swirl number:

$$S_g^* = S_g(D_e/D_0) \tag{4}$$

Due to this modification, the integral swirl number S (S_g*) is well generalized in logarithmic coordinates (Fig. 10b, the correlation coefficient R^2 is 95%). From this generalization, it can be concluded that for swirl parameters below the critical value $S_{crit} = 0.5$ (Gupta et al., 1984), the PVC effect is not detected in the flow (according to Table 1).

It can also be shown that by using constricting nozzles, the flow can be given the same degree of swirl. Fig. 11 shows completely similar velocity profiles for two different cases: 1) $S_g = 1.2$ and $D_e = 30$ mm and 2) $S_g = 0.9$ and $D_e = 40$ mm. Identical velocity profiles give the same value of the integral swirl number according to formula (2), which is close to the modified swirl number S_g*=0.474.

Now, for all flow configurations with PVC formation, we select the number Sh for a fixed value $Re = 5 \cdot 10^4$ according to the data from Fig. 6. The dependence of Sh on the modified swirl number S_g* is shown in

Table 1
Identification of a PVC for all flow configurations considered.

D_e, mm / S_g	30	40	52	76
0.3	–	–	–	+
0.6	–	+	+	+
0.9	+	+	+	–
1.2	+	+	+	–

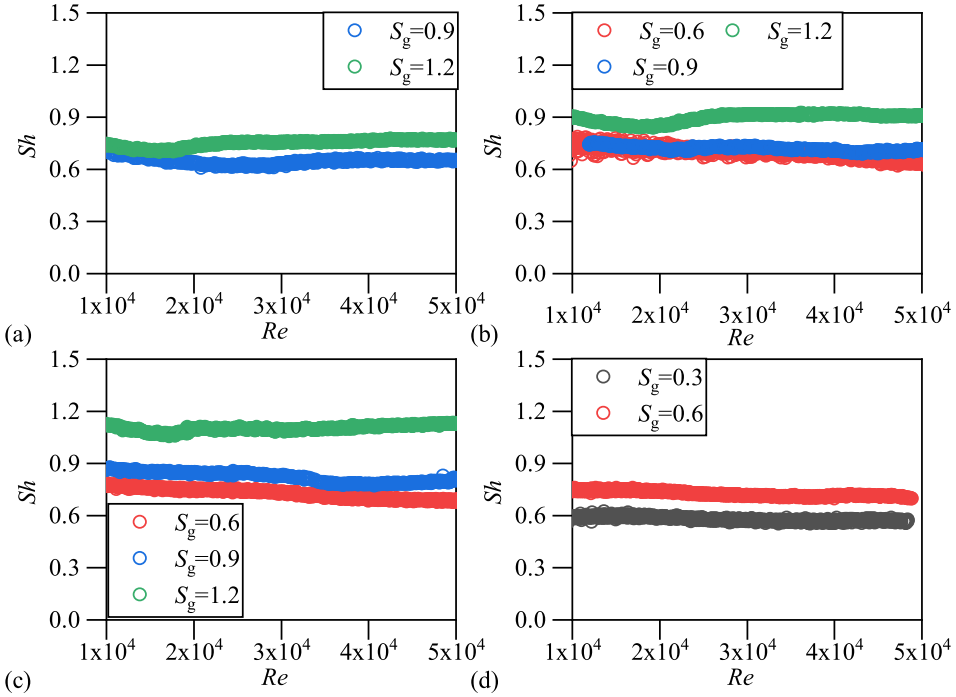

Fig. 6. Dependence of Sh on Re for different exit nozzles: (a) $D_e = 30$ mm, (b) $D_e = 40$ mm, (c) $D_e = 52$ mm, and (d) $D_e = 76$ mm.

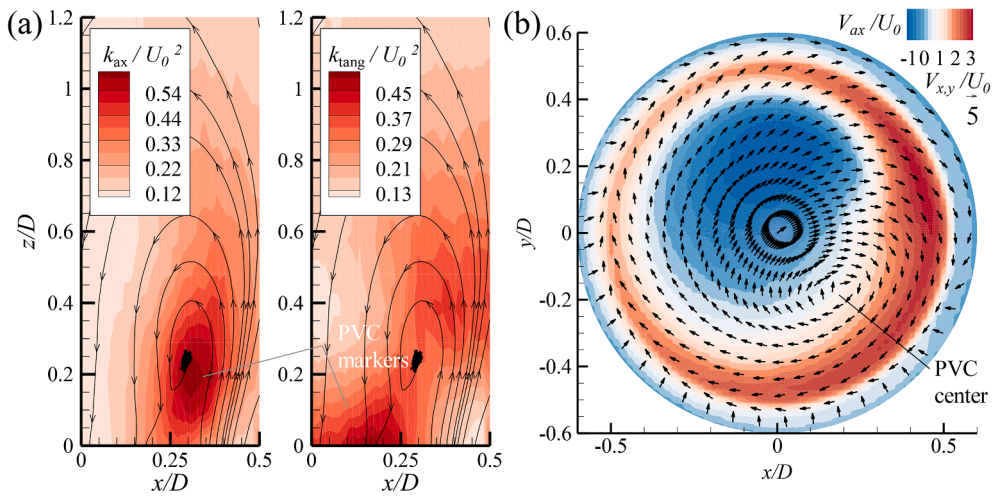

Fig. 7. Typical flow with a PVC for $D_e = 52$ mm and $S_g = 1.2$: (a) distributions of k/U_0^2 with streamlines, (b) phase-averaged velocity in the crosswise section.

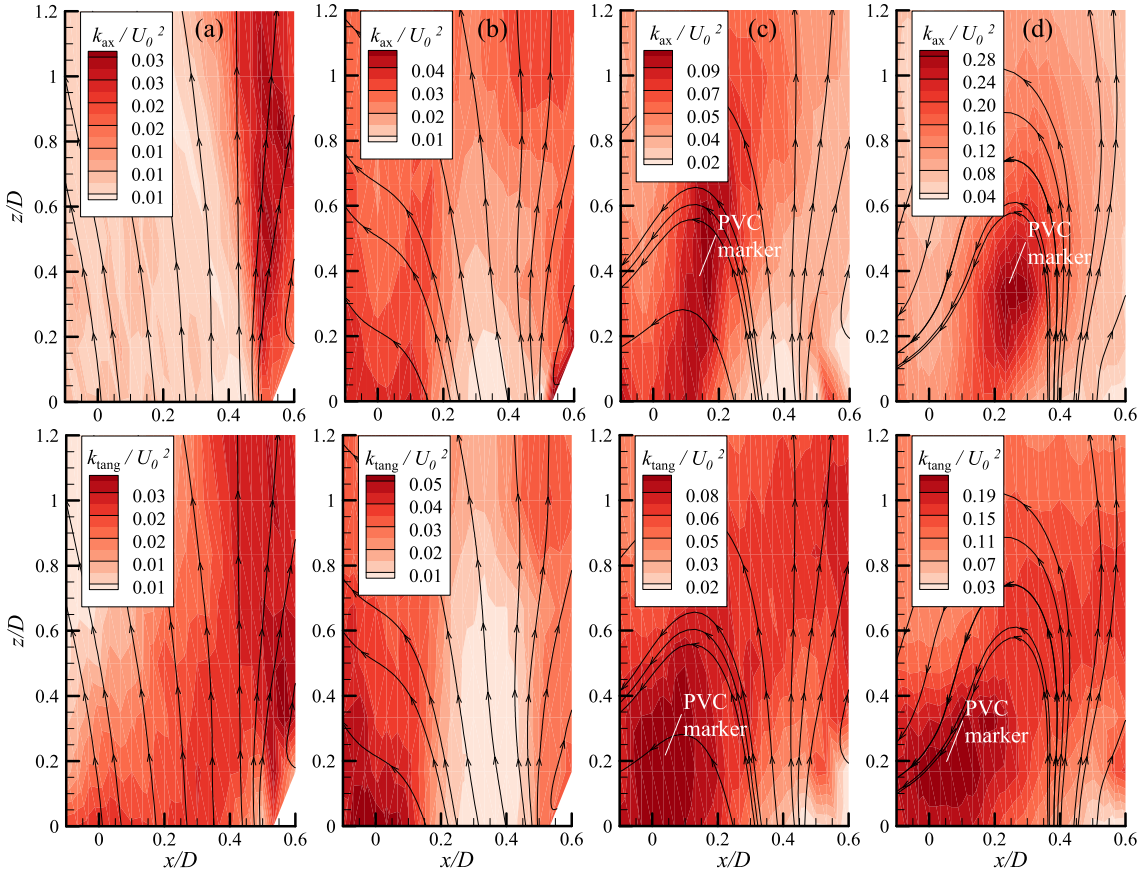

Fig. 8. Distributions of dimensionless TKE k/U_0^2 with streamlines for the nozzle with $D_e = 30$: (a) $S_g = 0.3$, (b) $S_g = 0.6$, (c) $S_g = 0.9$, and (d) $S_g = 1.2$.

Fig. 12. It is evident that this dependence is accurately linear, which allows us to generalize all the results obtained in this study to the class of vane swirlers. This empirical formula can be used to estimate the frequency in the initial design stage of swirl devices.

5. Conclusions

A parametric study of the swirl flow produced by a flat-vane swirler was performed for four vane angles and four exit nozzle diameters. It is shown that the conditions leading to the PVC effect at the exit of the swirler can be achieved by varying the vane angle and the diameter of the exit nozzle.

A clear link is found between the PVC induced pressure pulsations and the tangential velocity fluctuations measured by LDV. The use of microphones provides a quick way to measure the frequency response of the swirl flow in a wide range of geometries and flow configurations.

It is shown that by varying the vane angle and the diameter of the exit nozzle, it is possible to independently influence the swirl number

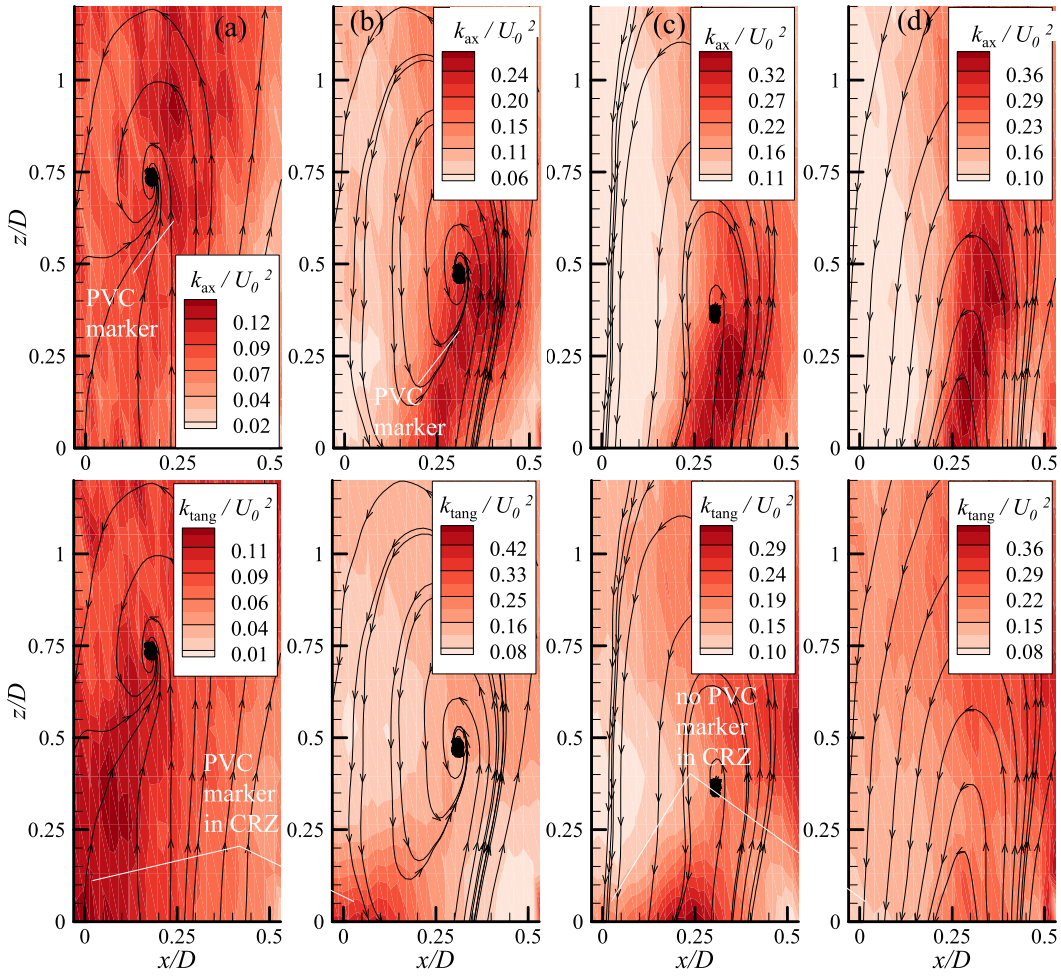

Fig. 9. Streamlines and profiles of axial velocity pulsations for a nozzle with $D_e = 76$ (without a constriction nozzle): (a) $S_g = 0.3$, (b) $S_g = 0.6$, (c) $S_g = 0.9$, and (d) $S_g = 1.2$.

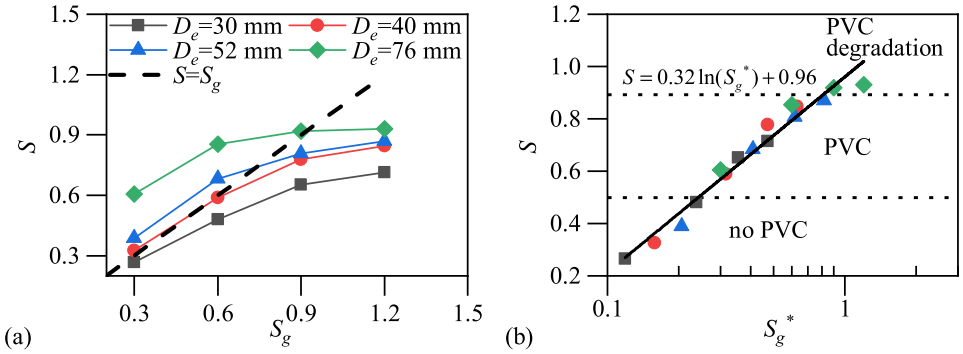

Fig. 10. Dependences of the integral swirl number S (Eq. 2) on the geometric swirl number S_g (a) and the modified geometric swirl number S_g* (b) (a log scale is used on the abscissa) for different diameters of the exit nozzle D_e = 30, 40, 52, and 76 mm.

and the formation of a precessing vortex core (PVC) at the exit of the swirler nozzle. It is found that a PVC does not occur at low $S_g = 0.3$ at small nozzle diameters (D_e = 30–52 mm) due to the subcritical swirl number $S < 0.5$, at which a PVC is not formed in the flow (Gupta et al., 1984). In the case of strong swirling flow (S_g = 0.9 and 1.2) in the absence of constriction by the nozzle ($D_e/D = 1$), the disappearance of the PVC effect due to the strong displacement of the flow to the chamber walls was observed. The absence of a PVC in the flow was proved by measuring the frequency response of the flow in a wide range of *Re* numbers and by the absence of specific markers in TKE distributions (or RMS distributions of velocity pulsations). We established two footprints of the PVC effect in TKE distributions: *i)* an M−shaped distribution of the axial contribution of TKE; *ii)* a central maximum in the distribution of the tangential contribution of TKE.

The possibility of generalizing the integral swirl number based on the modified geometric definition S_g^* containing the degree of flow constriction was shown using an empirical logarithmic dependence $S(S_g^*)$. A generalized linear dependence of the Strouhal number on the modified swirl number was obtained. Thus, a generalization of the fre-

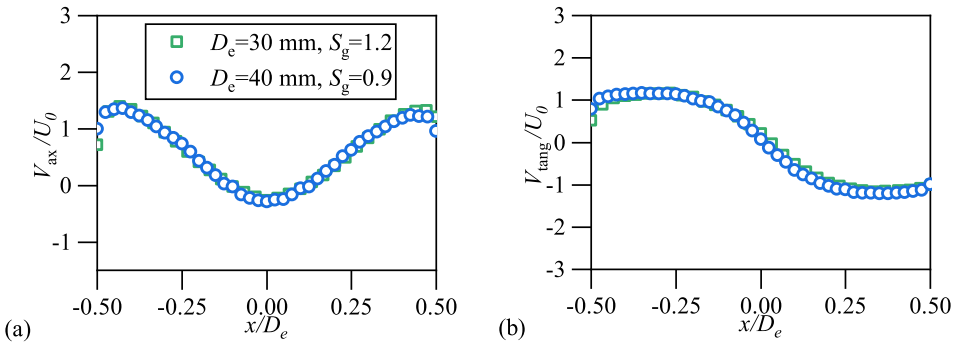

Fig. 11. Velocity profiles for two cases: $D_e = 30$, $S_g = 1.2$ and $D_e = 40$, $S_g = 0.9$.

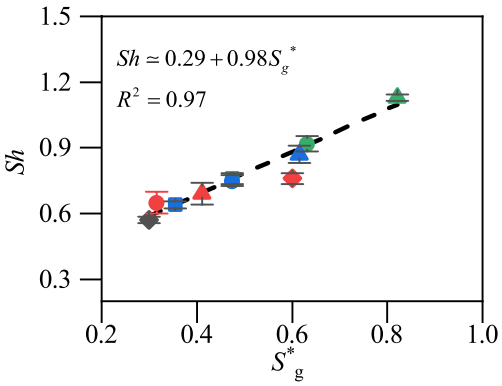

Fig. 12. Dependence of the *Sh* number as a function of the modified geometric swirl number S_g* (the point $S_g = 0.6$, $D_e = 76$ mm was excluded from the consideration because of its strong deviation from the linear dependence; the same symbols for different S_g as in Fig. 3).

quency characteristics of swirling flow with a PVC for the class of axial vane swirlers was performed. These results are highly relevant for engineering applications since they can be useful for predicting the frequency characteristics of flows with PVC formation.

Declaration of Competing Interest

The authors declare that they have no known competing financial interests or personal relationships that could have appeared to influence the work reported in this paper.

Acknowledgments

The authors acknowledge the support of the RFBR (No. 18-08-01467) for velocity and pressure measurements. I. Litvinov acknowledges the support of the RSF (No. 19-79-10225) for the empirical analysis of swirl flow. Setups and equipment were used within the framework of a state contract with IT SB RAS (Project No. 121031800229-1).

References

Akhmetov, D.G., Nikulin, V.V., Petrov, V.M., 2004. Experimental study of self-oscillations developing in a swirling-jet flow. Fluid Dyn. 39 (3), 406–413.
Al-Abdeli, Y.M., Masri, A.R., 2004. Precession and recirculation in turbulent swirling isothermal jets. Combust. Sci. Technol. 176 (5-6), 645–665.
Alekseenko, S.V., Kuibin, P.A., Okulov, V.L., Shtork, S.I., 1999. Helical vortices in swirl flow. J. Fluid Mech. 382, 195–243.
Anacleto, P.M., Fernandes, E.C., Heitor, M.V., Shtork, S.I., 2003. Swirl flow structure and flame characteristics in a model lean premixed combustor. Combust. Sci. Technol. 175 (8), 1369–1388.
Balakrishnan, P., Srinivasan, K., 2018. Influence of swirl number on jet noise reduction using flat vane swirlers. Aerosp. Sci. Technol. 73, 256–268.
Boxx, I., Stöhr, M., Carter, C., Meier, W., 2010. Temporally resolved planar measurements of transient phenomena in a partially pre-mixed swirl flame in a gas turbine model combustor. Combust. Flame 157 (8), 1510–1525.
Cala, C.E., Fernandes, E.C., Heitor, M.V., Shtork, S.I., 2006. Coherent structures in unsteady swirling jet flow. Exp. Fluids 40 (2), 267–276.
Candel, S., Durox, D., Schuller, T., Bourgouin, J.-F., Moeck, J.P., 2014. Dynamics of swirling flames. Annu. Rev. Fluid Mech. 46 (1), 147–173.
Cassidy, J.J., Falvey, H.T., 1970. Observations of unsteady flow arising after vortex breakdown. J. Fluid Mech. 41 (4), 727–736.
Chanaud, R.C., 1965. Observations of oscillatory motion in certain swirling flows. J. Fluid Mech. 21 (01), 111. https://doi.org/10.1017/S0022112065000083.
Chigier, N.A., Beér, J.M., 1964. Velocity and static-pressure distributions in swirling air jets issuing from annular and divergent nozzles. J. Basic Eng. 86, 788.
Chigier, N.A., Chervinsky, A., 1967. Experimental investigation of swirling vortex motion in jets. J. Appl. Mech. 34, 443–451.
Ciocan, G.D., Iliescu, M.S., Vu, T.C., Nennemann, B., Avellan, F., 2007. Experimental study and numerical simulation of the FLINDT draft tube rotating vortex. J. Fluids Eng. 129, 146–158.
Degenève, A., Jourdaine, P., Mirat, C., Caudal, J., Vicquelin, R., Schuller, T., 2019. Effects of a diverging cup on swirl number, flow pattern, and topology of premixed flames. J. Eng. Gas Turbines Power 141, 031022.
Derksen, J.J., Van den Akker, H.E.A., 2000. Simulation of vortex core precession in a reverse-flow cyclone. AIChE J. 46 (7), 1317–1331.
Ranga, K.R., Kirkpatrick, M.P., 2009. Study of jet precession, recirculation and vortex breakdown in turbulent swirling jets using LES. Comput. Fluids 38 (6), 1232–1242.
Dulin, V.M., Lobasov, A.S., Chikishev, L.M., Markovich, D.M., Hanjalic, K., 2019. On impact of helical structures on stabilization of swirling flames with vortex breakdown: flow. Turbul. Combust. 103 (4), 887–911.
Durox, D., Moeck, J.P., Bourgouin, J.-F., Morenton, P., Viallon, M., Schuller, T., Candel, S., 2013. Flame dynamics of a variable swirl number system and instability control. Combust. Flame 160 (9), 1729–1742.
Farokhi, S., Taghavi, R., Rice, E.J., 1989. Effect of initial swirl distribution on the evolution of a turbulent jet. AIAA J. 27 (6), 700–706.
Feikema, D., Chen, R.-H., Driscoll, J.F., 1990. Enhancement of flame blowout limits by the use of swirl. Combust. Flame 80 (2), 183–195.
Fernandes, E.C., Heitor, M.V., Shtork, S.I., 2006. An analysis of unsteady highly turbulent swirling flow in a model vortex combustor. Exp. Fluids 40 (2), 177–187.
Goyal, R., Cervantes, M.J., Gandhi, B.K., 2017. Vortex rope formation in a high head model Francis turbine. J. Fluids Eng. 139, 041102.
Griffiths, A.J., Yazdabadi, P.A., Syred, N., 1998. Alternate eddy shedding set up by the nonaxisymmetric recirculation zone at the exhaust of a cyclone dust separator: Journal of Fluids Engineering. Trans. ASME 120, 193–199.
Grimble, T.A., Agarwal, A., 2015. Characterisation of acoustically linked oscillations in cyclone separators. J. Fluid Mech. 780, 45–59.
Gupta, K., Lilley, D.G., Syred, N., 1984. Swirl Flows. Abacus Press.
Gursul, I., 1996. Effect of nonaxisymmetric forcing on a swirling jet with vortex breakdown. J. Fluids Eng. 118, 316–321.
Hee Lee, D., Youl Won, S.e., Taek Kim, Y., Suk Chung, Y., 2002. Turbulent heat transfer from a flat surface to a swirling round impinging jet. Int. J. Heat Mass Transf. 45 (1), 223–227.
Iliescu, M.S., Ciocan, G.D., Avellan, F., 2008. Analysis of the cavitating draft tube vortex in a francis turbine using particle image velocimetry measurements in two-phase flow. J. Fluids Eng. 130, 021105.
Khandelwal, B., Lili, D., Sethi, V., 2014. Design and study on performance of axial swirler for annular combustor by changing different design parameters. J. Energy Inst. 87 (4), 372–382.
Litvinov, I.V., Sharaborin, D.K., Shtork, S.I., 2019. Reconstructing the structural parameters of a precessing vortex by SPIV and acoustic sensors. Exp. Fluids 60, 139.
Litvinov, I.V., Shtork, S.I., Kuibin, P.A., Alekseenko, S.V., Hanjalic, K., 2013. Experimental study and analytical reconstruction of precessing vortex in a tangential swirler. Int. J. Heat Fluid Flow 42, 251–264.
Manoharan, K., Frederick, M., Clees, S., O'Connor, J., Hemchandra, S., 2020. A weakly nonlinear analysis of the precessing vortex core oscillation in a variable swirl turbulent round jet. J. Fluid Mech. 884, A29.
Martinelli, F., Olivani, A., Coghe, A., 2007. Experimental analysis of the precessing vortex core in a free swirling jet. Exp. Fluids 42 (6), 827–839.

Milosavljevic, V.D., Taylor, A.M.K.P., Whitelaw, J.H., 1990. The influence of burner geometry and flow rates on the stability and symmetry of swirl-stabilized nonpremixed flames. Combust. Flame 80 (2), 196–208.
Moeck, J.P., Bourgouin, J.-F., Durox, D., Schuller, T., Candel, S., 2012. Nonlinear interaction between a precessing vortex core and acoustic oscillations in a turbulent swirling flame. Combust. Flame 159 (8), 2650–2668.
Mohammadi, M., Hajidavalloo, E., Behbahani-Nejad, M., 2019. Investigation on Combined Air and Water Injection in Francis Turbine Draft Tube to Reduce Vortex Rope Effects. J. Fluids Eng. 141, 051301.
Oberleithner, K., Sieber, M., Nayeri, C.N., Paschereit, C.O., Petz, C., Hege, H.-C., Noack, B.R., Wygnanski, I., 2011. Three-dimensional coherent structures in a swirling jet undergoing vortex breakdown: stability analysis and empirical mode construction. J. Fluid Mech. 679, 383–414.
Pasche, S., Avellan, F., Gallaire, F., 2017. Part load vortex rope as a global unstable mode. J. Fluids Eng. 139, 051102.
Pausch, K., Herff, S., Schröder, W., 2020. Noise sources of an unconfined and a confined swirl burner. J. Sound Vib. 475, 115293. https://doi.org/10.1016/j.jsv.2020.115293.
Rajan, G.K., Cimbala, J.M., 2017. Computational and theoretical analyses of the precessing vortex rope in a simplified draft tube of a scaled model of a Francis turbine. J. Fluids Eng. 139, 021102.
Sheen, H.J., Chen, W.J., Jeng, S.Y., Huang, T.L., 1996. Correlation of swirl number for a radial-type swirl generator. Exp. Therm Fluid Sci. 12 (4), 444–451.
Shtork, S.I., Cala, C.E., Fernandes, E.C., 2007. Experimental characterization of rotating flow field in a model vortex burner. Exp. Therm Fluid Sci. 31 (7), 779–788.
Shtork, S.I., Vieira, N.F., Fernandes, E.C., 2008. On the identification of helical instabilities in a reacting swirling flow. Fuel 87 (10-11), 2314–2321.
Shtork, S.I., Comas, O., Fernandes, E.C., Heitor, M.V., 2005. Aerodynamic structure of unsteady swirling flow downstream of a sudden expansion. Thermophys. Aeromech. 2, 217–228.
Skripkin, S., Tsoy, M., Shtork, S., Hanjalić, K., 2016. Comparative analysis of twin vortex ropes in laboratory models of two hydro-turbine draft-tubes. J. Hydraul. Res. 54 (4), 450–460.
Stöhr, M., Sadanandan, R., Meier, W., 2011. Phase-resolved characterization of vortex–flame interaction in a turbulent swirl flame. Exp. Fluids 51 (4), 1153–1167.
Syred, N., 2006. A review of oscillation mechanisms and the role of the precessing vortex core (PVC) in swirl combustion systems. Prog. Energy Combust. Sci. 32 (2), 93–161.
Syred, N., Beér, J.M., 1974. Combustion in swirling flows: a review. Combust. Flame 23 (2), 143–201.
Syred, N., Gupta, A.K., Beér, J.M., 1975. Temperature and density gradient changes arising with the precessing vortex core and vortex breakdown in swirl burners. Symp. (Int.) Combust. 15 (1), 587–597.
Toh, I.K., Honnery, D., Soria, J., 2010. Axial plus tangential entry swirling jet. Exp. Fluids 48 (2), 309–325.
Tropea, C., Yarin, A.L., Foss, J.F. (Eds.), 2007. Springer Handbook of Experimental Fluid Mechanics. Springer Berlin Heidelberg, Berlin, Heidelberg.
Valera-Medina, A., Syred, N., Griffiths, A., 2009. Visualisation of isothermal large coherent structures in a swirl burner. Combust. Flame 156 (9), 1723–1734.
Yang, J., Dong, Z., Shen, C., Zhang, W., Hao, X., Guan, G., 2019. Analysis of effect of radial confluence flow on vortex core motion. Powder Technol. 356, 871–879.
Yanta, W.J., Smith, R.A., 1978. Measurements of turbulence-transport properties with a laser Doppler velocimeter: AIAA Paper 73–169 -. American Institute of Aeronautics and Astronautics, 11th Aerospace Sciences Meeting.
Yazdabadi, P.A., Griffiths, A.J., Syred, N., 1994. Characterization of the PVC phenomena in the exhaust of a cyclone dust separator. Exp. Fluids 17 (1-2), 84–95.
Zakharov, D.L., Krasheninnikov, S.Y., Maslov, V.P., Mironov, A.K., Toktaliev, P.D., 2014. Investigation of unsteady processes, flow properties, and tonal acoustic radiation of a swirling jet. Fluid Dyn. 49 (1), 51–62.